Icarus **145**, 122–139 (2000)
doi:10.1006/icar.1999.6319, available online at http://www.idealibrary.com on IDEAL®

Integrated Spectral Analysis of Mare Soils and Craters: Applications to Eastern Nearside Basalts

Matthew I. Staid and Carle M. Pieters

Department of Geological Sciences, Box 1846, Brown University, Providence, Rhode Island 02912
E-mail: matthew_staid@brown.edu

Received December 23, 1998; revised October 22, 1999

High spatial resolution Clementine images are examined to measure the reflectance properties of small and optically immature mare craters that have sampled discrete compositional units. The spectral properties of these relatively crystalline mare materials are compared to associated mature soils to determine the effects of space weathering on specific basalt types. Space weathering is observed to alter the optical properties of distinct lunar basalt units in a systematic manner allowing compositional distinctions to be recognized across maturity states. Ultraviolet/visible reflectance properties of mare basalts are sensitive to titanium content but are relatively independent of maturity state and demonstrate only a slight reddening as regoliths mature to soils. Other compositional distinctions between basalt types are identified by differences in albedo and band strength of ferrous minerals that are maintained over a full range of maturity states. Immature deposits within large craters are compared to the spectral properties of well-defined mare units to examine the composition of buried materials. When craters excavate through the mare, highland contamination is readily identified as a mixing relation between mafic and feldspathic lithologies. The approach presented here provides new information on the composition and stratigraphy of several nearside mare deposits, including the identification of thin low-iron and very low titanium basalts in Lacus Somniorum and more iron-rich low-titanium basalts in eastern Mare Frigoris.

Key Words: **moon; spectroscopy; volcanism; regoliths; cratering.**

INTRODUCTION

Remote studies of the lunar surface have extended our knowledge of mare basalt types beyond those sampled at the Apollo and Luna landing sites. Telescopic measurements have provided particularly important information about unsampled mare regions based on albedo and visible to near-infrared absorption features exhibited by mature mare soils (e.g., Pieters and McCord 1976, Johnson *et al.* 1977, Matson *et al.* 1977, Pieters 1978, 1993, Adams *et al.* 1981, Johnson *et al.* 1991a). Telescopic mapping of four compositionally sensitive spectral parameters (UV/VIS ratio, albedo, 1-μm band strength, and 2-μm band strength) have been used to distinguish 13 mare basalt types and three additional lunar volcanic groups (Pieters 1978). Such studies have established the distribution of volcanic materials across the lunar nearside and suggest that the majority of the observed basalts are not represented in the returned samples (Pieters 1978). This classification of mare soils was extended to include farside basalts through studies of Mariner 10 multispectral images (Robinson *et al.* 1992), the interpretation of Galileo solid-state imaging (SSI) multispectral data (Greeley *et al.* 1993, Kadel *et al.* 1992, Williams *et al.* 1993), and most recently Clementine data (Pieters *et al.* 1995a, Hiesinger *et al.* 1996, Merenyi *et al.* 1997). The spatial and stratigraphic distribution of spectrally distinct mare units indicates that lunar volcanism was complex and that basin-scale magmatism evolved independently within neighboring regions (Pieters 1993, Hiesinger *et al.* 1998).

Though all mature mare soils display a characteristic red lunar continuum slope, small differences in relative color and near-infrared absorptions have been used to estimate the composition of lunar volcanics. Early telescopic measurements of Apollo and Luna landing sites showed that ilmenite rich regions of the lunar maria have a flatter continuum slope in the visible wavelengths (and are therefore bluer) than sites which sampled lower titanium mare soils. Subsequently, laboratory reflectance measurements of returned lunar soils resulted in more quantitative relations between reflectance properties and composition. Charette *et al.* (1974) documented an empirical relationship between the ultraviolet to visible ratio of mature mare soils and their titanium content. Near-infrared absorption bands observed in mare soils near 1 and 2 μm also provide mineralogical information related to the composition and the abundance of high-Ca pyroxene (Adams 1974, Cloutis and Gaffey 1991, Burns 1993). Variations observed in the relative width of the 1-μm band are believed to be produced by additional soil components with absorption band centers at longer wavelengths, such as olivine and glass (Pieters *et al.* 1980, McCord *et al.* 1981).

A significant amount of information about the diversity of lunar basalt types has been obtained from remote observations of unsampled mare regions. However, mineralogic and compositional interpretation of unsampled units is complicated by the effects of space weathering and nonmare contamination as regoliths mature to soils in the space environment. As a result, it is often difficult to determine the composition of emplaced

0019-1035/00 $35.00

basaltic materials from spectral measurements of optically weathered surface soils. In contrast, the approach initiated here emphasizes examination of relatively crystalline materials excavated by small craters in the maria. This approach circumvents many of the issues associated with multicomponent well developed soils and directly addresses the character of emplaced basalts.

The Clementine ultraviolet–visible (UVVIS) camera acquired multispectral images of the whole Moon during 2 months of lunar mapping in 1994 (Nozette *et al.* 1994). Clementine's UVVIS camera contained five filters centered at 415, 750, 900, 950, and 1000 nm. The wavelength positions of these filters were chosen to maximize the mineralogic information obtainable within this spectral region by characterizing the ultraviolet/visible slope and the strength and shape of the 1-μm ferrous band. The high spatial resolution of the UVVIS instrument (~100–200 m/pixel) resolved mare crater deposits small enough to sample individual volcanic flows (Staid and Pieters 1996). These freshly exposed materials are significantly less affected by space weathering and are therefore important sites for the remote assessment of basalt petrology. Five-color spectra are examined both as a function of crater size and by isolating the least weathered materials within a given unit. Results are compared with the optical properties of mature soils and previous telescopic classification. Since craters excavate material from a depth proportional to their size, mare crater deposits also provide information about the thickness and stratigraphy of lunar volcanic units. This initial study of lunar basalt types focuses on several eastern nearside mare units. The approach will later be expanded to include other near and farside basalt types.

PREVIOUS WORK AND ISSUES

The eastern nearside contains some of the most diverse and extensively studied mare regions on the Moon. The adjacent Tranquillitatis and Serenitatis basins also include the only two Apollo sites to have sampled high-titanium basalts: Apollo 11 and 17. The locations of the eastern nearside maria and landing sites are provided on a USGS mosaic of Clementine images in Fig. 1. For reference, Pieters' 1978 spectral classifications of these mare units are also provided.

The border of the high titanium Tranquillitatis basalts and the voluminous and younger Serenitatis basalts form a prominent color boundary on the lunar nearside. To the south, basalts within Tranquillitatis are relatively blue compared to most other regions of the Moon. Maps of soil titanium content derived from empirical optical studies suggest that soils within Tranquillitatis contain some of the highest titanium abundances on the lunar nearside (e.g., McCord *et al.* 1976, 1979, Johnson *et al.* 1977, Pieters 1978, Johnson *et al.* 1991a, Melendrez *et al.* 1994). These titanium maps are in close agreement with studies of orbital gamma ray data (Metzger and Parker 1979, Davis 1980).

Detailed studies of Mare Tranquillitatis have shown that its basalts are relatively thin and are composed of several layers which vary in composition and thickness, increasing somewhat in titanium content for the younger flows (Melendrez *et al.* 1994, Staid *et al.* 1996). Though thin, the stratigraphic units within Tranquillitatis are observed to be areally extensive. Interpretation of remotely acquired data within Tranquillitatis has greatly benefited from the proximity of the Apollo sampling sites and studies of the returned samples. One young high titanium unit extending across the entire basin (Tvh-B unit, Staid *et al.* 1996)

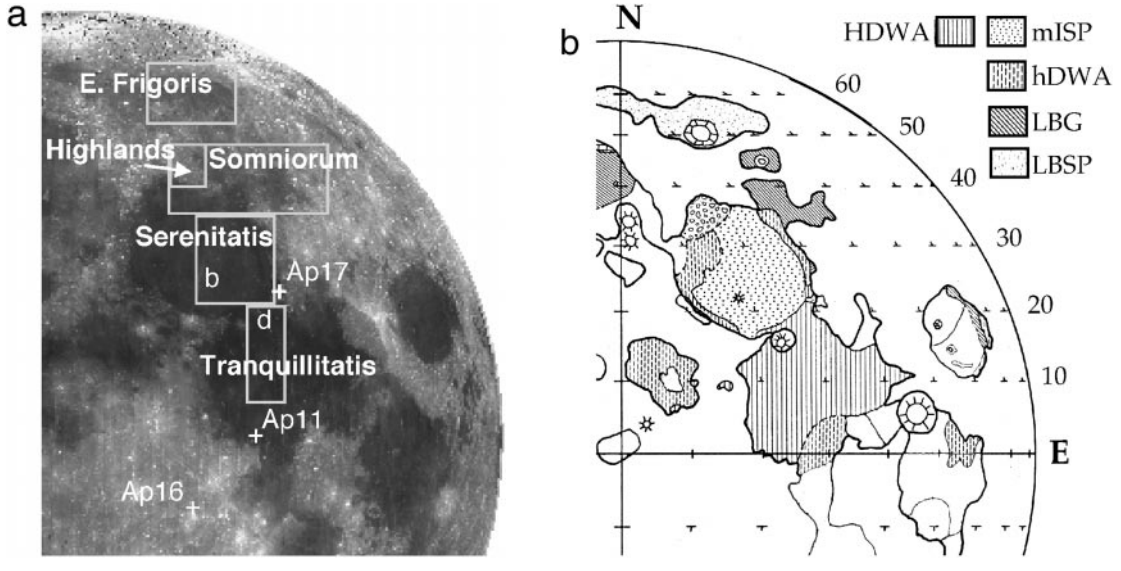

FIG. 1. (a) The eastern near-side of the Moon as seen in a Clementine 0.75-μm USGS global mosaic showing the location of several nearside maria and Apollo landing sites. The general locations of each study region discussed in the text are outlined with rectangles. The location of Dawes crater (18 km) in Mare Tranquillitatis and Bessel crater (16 km) in Mare Serenitatis are indicated by the symbols d and b, respectively. (b) Telescopic classification of basalt types from Pieters (1978) relevant to this study.

may be a source of high-titanium, low potassium basalts sampled at both Apollo 11 and Apollo 17 (Snyder *et al.* 1992, 1994). The youngest and highest titanium basalt observed in Tranquillitatis is believed to be sampled only at Apollo 11 (Staid *et al.* 1996).

On the northern side of the boundary, mare deposits in Serenitatis are relatively red and have been interpreted as low to very low titanium with strong near-infrared absorptions resulting from a high iron content (Pieters 1978, Bell and Hawke 1995). The majority of Serenitatis deposits were classified into a single basalt-type unit (mISP) by telescopic studies (Pieters, 1978) and are younger than Tranquillitatis basalts, forming a stratigraphic contact with these older deposits along the southern border (Howard *et al.* 1973). A second Serenitatis unit on the eastern border of the basin (hDWA, Pieters 1978, Fig. 1) is lower in albedo and has slightly bluer UV–VIS spectral properties. The Apollo 17 mission to the Serenitatis basin massifs near the border of Tranquillitatis and Serenitatis returned a variety of high and low-Ti basalts as well as pyroclastic dark mantling materials.

Mare deposits within Lacus Somniorum to the northeast of Serenitatis (Fig. 1) consist of unusually bright and red mare soils. The compositional properties of these unsampled mare units are ambiguous. The very red UV/VIS spectral properties and high overall albedo of the Lacus Somniorum region may result from the emplacement of a distinct very low titanium unit (Pieters 1978). Alternatively, these mare deposits may have been similar to the adjacent Serenitatis basalts when emplaced then exposed to significant reddening and brightening from highland contamination (Fischer and Pieters 1995).

Mare Frigoris' soils, located to the north and west of Serenitatis, are also very bright and red compared to other nearside maria. Initial telescopic characterization of the Frigoris, region identified a prominent 1-μm band in mature soils within Frigoris, suggesting that the basaltic soils of this vast region are iron rich (Pieters 1978). On the other hand, studies of multispectral images using recent models for iron mapping have suggested that the vast plains of Frigoris may represent low-Fe mare deposits (Taylor *et al.* 1996, Lucey *et al.* 1998a).

The spectral properties of relatively crystalline and optically immature craters provide an additional source of information to evaluate and characterize the composition of emplaced basaltic materials. Lunar craters are thought to be the best analog for laboratory measurements of particulate samples of lunar rocks exhibiting the most diagnostic absorption features related to sample mineralogy (e.g., McCord and Adams 1973, Burns 1993). Mafic lunar minerals are relatively insensitive to shock effects and maintain their diagnostic absorption features up to the point of melting (Adams *et al.* 1979, Pieters 1993). However, the low spatial resolution of previous telescopic data has largely limited the spectral characterization of mare craters to those larger than 5 km in diameter which are likely to have excavated multiple subsurface units (Pieters 1993). As a result, previous data has not resolved the spectral properties of craters small enough to have sampled individual basalt flows or fresh exposures of basaltic stratigraphy within crater walls.

DATA ANALYSIS

Mare regions were investigated using Clementine UVVIS data of mare craters and soils. The five-band imagery requires extensive processing for calibration to produce multispectral image mosaics (Pieters *et al.* 1994). The following steps were used in calibrating each frame to derive bidirectional reflectance and are discussed in detail in Pieters *et al.* (1995b) and McEwen *et al.* (1998): (1) an offset correction based on the camera's electronic setting, (2) correction for dark current as a function of exposure time, temperature, and CCD row position, (3) a column dependent electronic shutter correction, (4) a flat field correction for spatial nonuniformity, (5) photometric corrections to a standard viewing geometry of 30°, and (6) spectral calibration to bidirectional reflectance using the Apollo 16 site as a lunar standard. A correction for the filter-to-filter effects of viewing

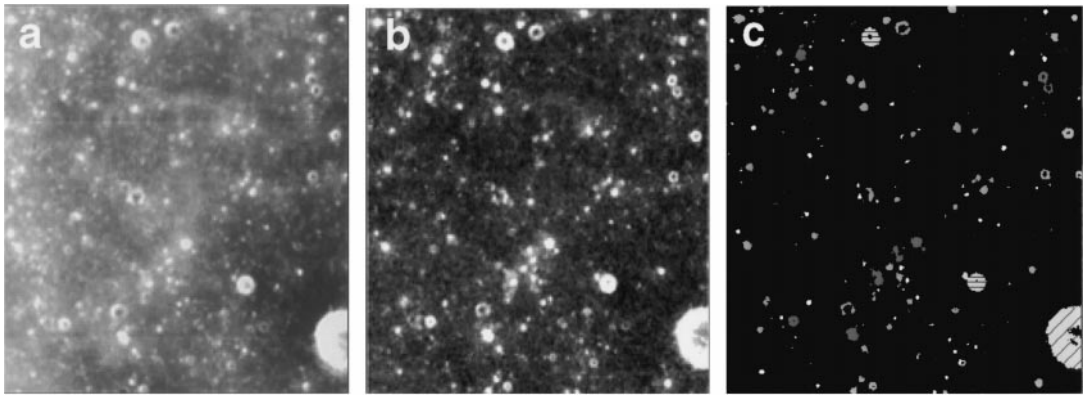

FIG. 2. Image processing steps performed to sample immature mare crater spectra. (a) Five-band Clementine images are calibrated and geometrically corrected (0.75-μm image of central Serenitatis shown here). (b) 0.75/1.0-μm Clementine image ratio is used to identify materials with strong 1-μm absorptions relative to surrounding soils. (c) Craters representing the 6% of materials with the strongest 1-μm bands are grouped by size. In this figure, craters assigned to the same size bin are marked with a common stipple pattern.

geometry developed by McEwen *et al.* (1998) was also applied to the Clementine data. Multispectral image cubes were then mosaicked into 10° latitude regions from which spectra of small regions were extracted. Large regions of each mare study area were also examined with useful spectral parameters to evaluate mare materials over a range of maturity states.

Five-color spectra were collected for hundreds of fresh craters of various sizes to create a large database for each mare region. Figure 2 illustrates the steps performed to isolate immature mare craters for each study area and group them based on size. In the first step (a), Clementine images of each mare region were calibrated and mosaicked as discussed in the previous section. All images were registered to USGS Clementine 0.75-μm base maps and resampled to 100 m spatial resolution. In the second step (b), a ratio of the 0.75/1.0 μm Clementine filters was used to identify materials exhibiting the strongest 1-μm absorptions relative to surrounding soils. In order to select many craters from each unit in an unbiased manner, the 6% of materials in a given unit with the strongest 1-μm ratio were used to identify immature materials. This threshold was identified independently for each mare unit and was used to isolate materials associated with individual fresh craters while minimizing the inclusion of overlapping ejecta blankets of adjacent craters. In the third step (c), a pattern recognition procedure was used to identify and bin fresh craters based on their estimated diameter. For each unit, results contain statistics from hundreds of craters within the smaller size bins (<0.5, 0.5–1, 1–2 km) and tens of craters or less in the largest bins (2–3, 3–5, 5+ km). The number of craters sampled as a function of size is provided for each unit in Table I and crater spectra are presented in Fig. 3. Previous mare soil unit designations of Pieters (1978) are used for comparison. The number of craters within the smallest bin size (<0.5) for Mare Tranquillitatis is unusually large for the area examined because of the many Dawes secondaries within the northern portion of the study region. Table I also provides the number of "immature" pixels at 100 m spatial resolution sampled from each mare unit. These pixels exhibit the highest combined 0.75-μm albedo and 1-μm strength from each mare region and were averaged to characterize the most "immature" materials within each basalt type.

Mare stratigraphic columns usually consist of many flows and are estimated to be 100s of meters to several kilometers in cumulative thickness (e.g., DeHon and Waskom 1976, Horz 1978, Sjogren *et al.* 1974, Solomon and Head 1980). Individual mare flows are believed to be much thinner, perhaps only tens of meters in thickness (e.g., Schaber 1973, Head 1976). The craters in the smallest size bins are therefore useful for characterizing the spectral properties of the uppermost mare units. In some cases, craters larger than several kms in diameter may be used to explore the stratigraphy of underlying units. Images of diagnostic spectral parameters were also examined to evaluate the properties of such craters spatially.

Calibrated images of each study area were also used to create scatter plots of several useful spectral parameters. To allow direct comparisons between regions these scatter plots were constructed by sampling 100,000 evenly spaced pixels from each mare region within areas indicated by white boxes in Fig. 1. The surface area of each study region sampled is provided in Table I. Areas of spectrally distinct continous ejecta around several craters (e.g., >10 km) were eliminated from the mare study regions to avoid sampling ejecta materials from subsurface units with a different composition. Scatter plots of the mare study areas are shown in Fig. 4. For comparison, highland materials from an area near Lacus Somniorum are also included in these plots. The intensity of each pixel within the scatter plots displays the relative abundance of data points containing a given value in the parameter space. Since mature soils dominate the surfaces exposed, the density distribution of each cloud has been presented

TABLE I
Mare Study Regions

Mare unit and type[a]	Diameter (km)	Symbol	No. of craters
T	Mature soils	■	
N Transquillitatis	<0.5	▽	~2550
	0.5–1	△	192
Type: HDWA	1–2	◇	41
Area = 5,796 km^2	2–3	❍	4
	3–5	□	1
	5+		
	Immature	X	28 Pixels
Sc	Mature soils	■	
Central Serenitatis	<0.5	▽	~2900
	0.5–1	△	~1040
Type: mISP	1–2	◆	306
Area = 27,070 km^2	2–3	❍	17
	3–5	□	7
	5+		1
	Immature	X	31 Pixels
Sb	Mature soils	■	
Serenitatis border	<0.5	▽	~450
	0.5–1	△	~140
Type: hDWA	1–2	◇	33
Area = 5,793 km^2	2–3	❍	3
	3–5	□	0
	5+		1
	Immature	X	45 Pixels
Sm	Mature soils	■	
Lacus Somniorum	<0.5	▽	~600
	0.5–1	△	~320
Type: LBG-	1–2	◇	172
Area = 17,660 km^2	2–3	❍	36
	3–5	□	9
	5+		3
	Immature	X	40 Pixels
Fr	Mature soils	■	
Eastern Frigoris	<0.5	▽	~2010
	0.5–1	△	~660
Type: LBG-	1–2	◇	173
Area = 18,617 km^2	2–3	❍	23
	3–5	□	8
	5+		0
	Immature	X	30 Pixels

[a] Pieters 1978.

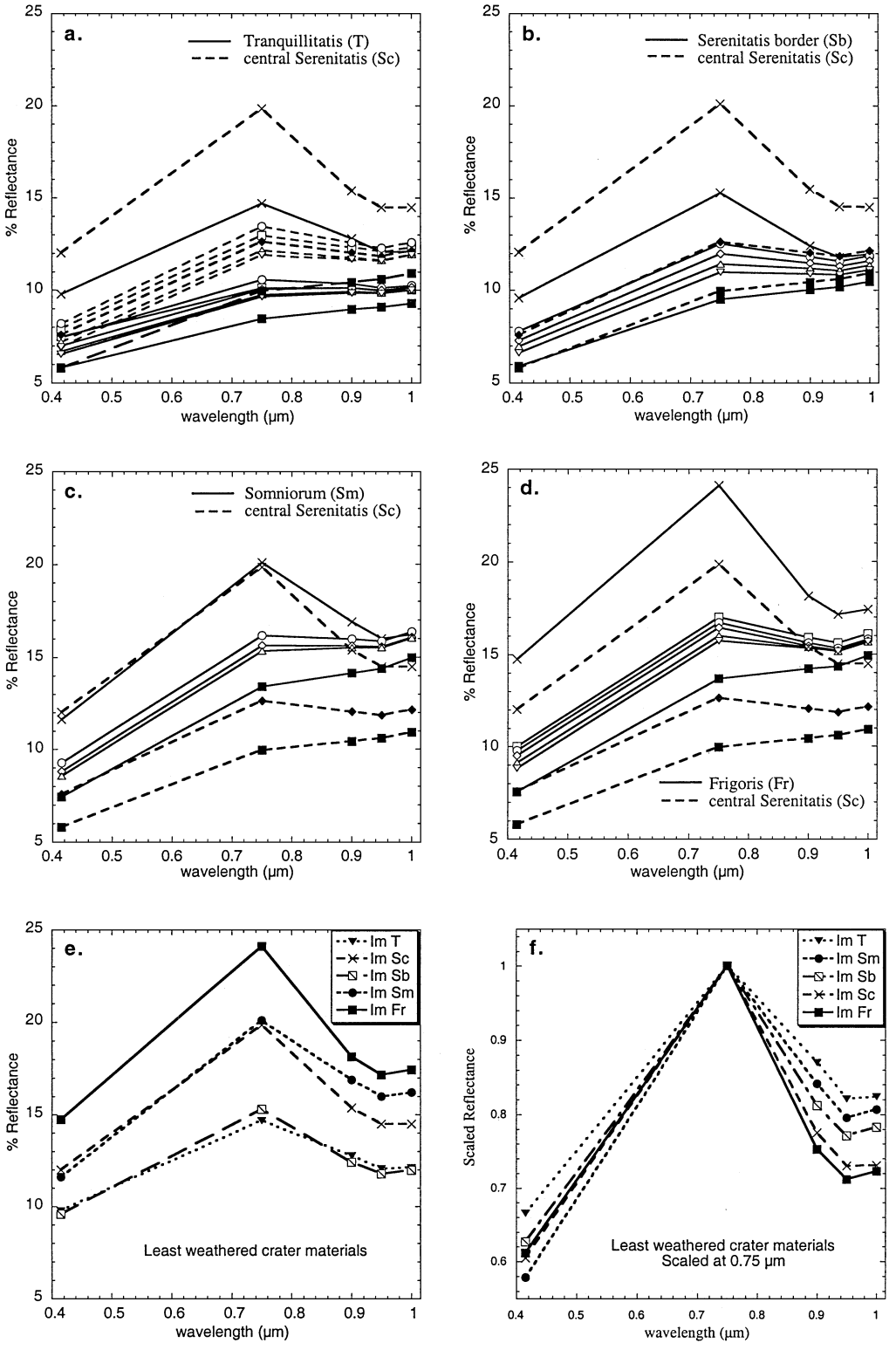

FIG. 3. (a–f) Five-color Clementine spectra for each mare region obtained by averaging all craters for each size bin. For comparison, representative central Serenitatis spectra are included in b, c, and d. Spectra of mature soils (average 9 × 9 pixel homogeneous areas or 0.81 km^2) and the most immature materials are also shown. The number of craters averaged for each size bin as well as symbol legends and the size of each study region is provided in Table I. Average standard deviations for the mature soil spectra and least weathered crater materials are 0.13 and 0.35% reflectance, respectively. Standard deviations crater group spectra vary with region and size, averaging 0.6% for smaller craters to 1.1% for the larger size groups.

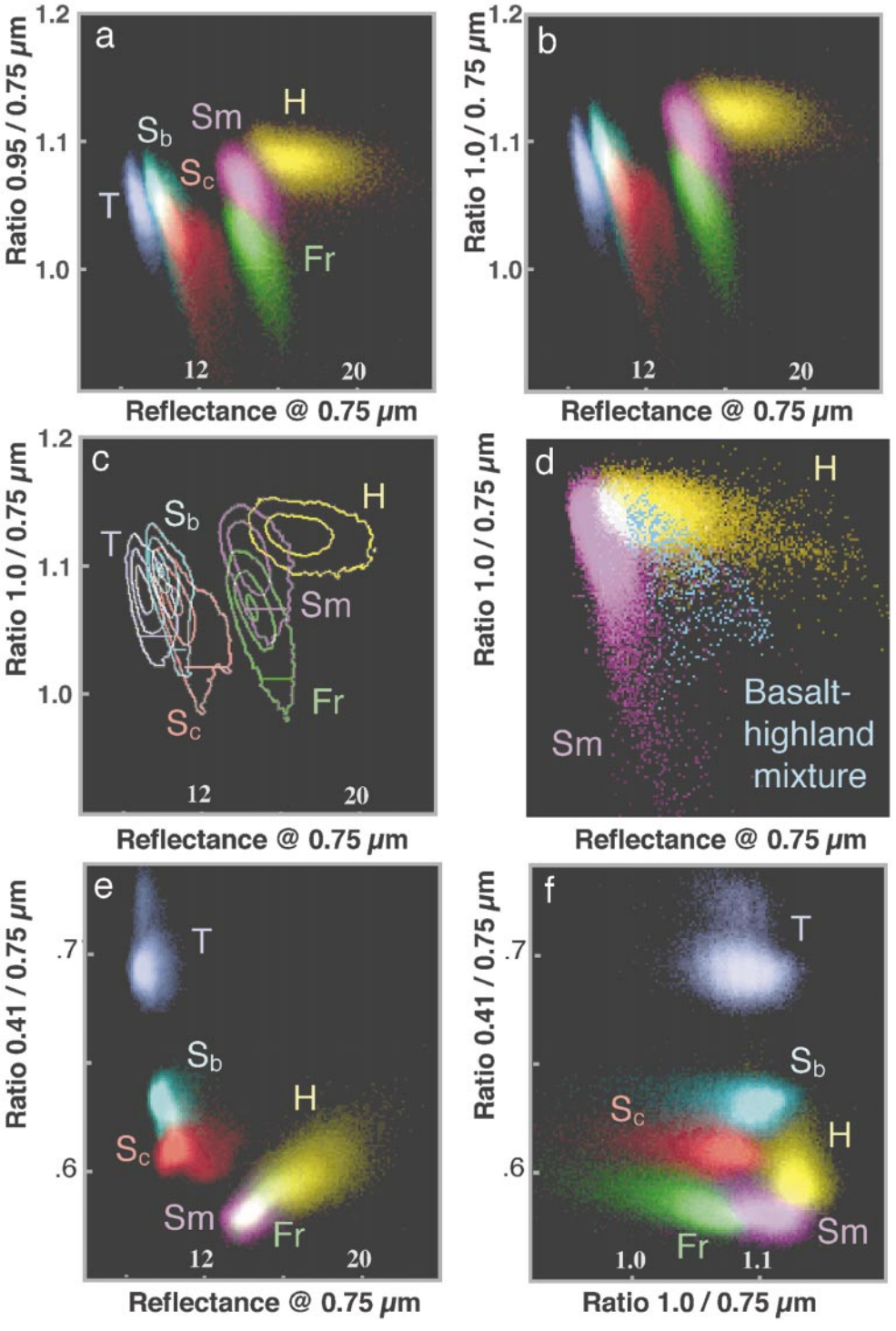

FIG. 4. Scatter plots of spectral parameters for mare study regions: Mare Tranquillitatis (T), the central and border regions of Serenitatis (Sc and Sb), Lacus Somniorum (Sm), and Mare Frigoris (Fr). For comparison, Highland materials (H) from an area near Lacus Somniorum are also included. A root stretch is used to enhance the visibility of less abundant immature materials. (a) Mafic absorption (0.95/0.75-μm ratio) vs albedo (0.75-μm reflectance). (b) Mafic absorption (1.0/0.75-μm ratio) vs albedo (0.75-μm reflectance). (c) Contoured scatter plot of the data in (b) to show the relative density each cloud. The 6% volume threshold used to identify immature craters is shown as a solid line across each mare unit. Contours occur at relative densities of 1, 10, 40, and 80% of the maximum density value. (d) Subset of scatter plot (b) with additional spectral properties of a 3.5-km Somniorum crater (blue) that exhibits vertical excavation of highland materials mixed with local basalts. (e) 0.41/0.75-μm ratio vs 0.75-μm reflectance. High titanium mare basalts from within Tranquillitatis are in the upper left. (f) 0.41/0.75-μm ratio vs mafic absorption ratio commonly used for standard false color composites of Clementine and Galileo images to distinguish different units.

after applying a square-root stretch to the intensity of each pixel. Plotting the square root of the density distribution enhances the visibility of the less abundant immature materials in the scatter plots. Areas where the spectral properties of more than one basalt type overlap result in brighter white regions within the scatter plots.

Exposure to space weathering weakens absorption features over time and the freshest and least weathered materials within a given unit exhibit the strongest absorption bands. A scatter plot of the 0.95/0.75-μm ratio and 0.75-μm reflectance (Fig. 4a) allows trends related to maturity to be evaluated (Fischer and Pieters 1996, Lucey *et al.* 1998a). Within a given basalt type, the most immature materials occur at the strongest 1-μm band strength (low values of 0.95/0.75-μm ratio) and highest 0.75-μm reflectance, i.e., toward the lower right of each data cloud. Immature materials and mature soils can be compared to determine how each unit alters optically as it weathers from relatively crystalline regolith to homogeneous soils.

Some Clementine spectra have been observed to contain a small "kink" between the 0.95- and the 1.0-μm filters for which scattered light has been suggested as a potential source (e.g., Pieters *et al.* 1995b). The 0.95 filter was of principal concern because its value relative to the 0.9- and 1.0-μm filters often appeared to be lower. In the event that there are scattered light effects which influence the relative position of the 0.95 and 1.0 filters, a plot of the 1.0/0.75-μm ratio versus 0.75-μm reflectance is provided in Fig. 4b for comparison. This parameter provides an alternate but comparable estimate of the 1-μm band strength consistent with the more commonly used 0.95/0.75-μm ratio. Both scatter plots (Figs. 4a and 4b) produce the same trends of roughly parallel weathering clouds for the basalt types studied. Since the Clementine data of each study area contains data from adjacent orbits with different viewing geometries, any remaining effects of viewing geometry on the position of data within the scatter plot would be seen as multiple trend for each compositional type. The scatter plots do not demonstrate any such errors resulting from differences in viewing geometries across orbits, nor are any systematic latitudinal differences seen in the data.

The scatter plot in Fig. 4b was contoured to determine the relative limits of each data cloud and the resulting map is presented in Fig. 4c. The 1-μm vs 0.75-μm scatter plots were also used to identify materials that represent the *most* immature materials within the study area of each mare unit. These areas were selected by identifying pixels within each study region that corresponded to the lower right limit of each mare unit's 1-μm vs 0.75-μm scatter plot cloud. Spectra of these materials were then compared to averaged spectra from crater size groups and mature soils.

Larger craters in some regions were clearly seen to have excavated through surface flows exposing materials with different spectral properties than overlying units. Scatter plot 4d compares the spectral properties of a Somniorum crater associated with the vertical excavation of highland with the optical properties of uncontaminated mare and highlands. This example is discussed in detail in a subsequent section on mare–highland mixing.

The UV/VIS ratio has been used extensively to estimate titanium in mature soils (e.g., Charette *et al.* 1974) and plots of this parameter against 0.75-μm reflectance are included for each unit in Fig. 4e. The UV/VIS ratio coupled with the 0.75-μm parameter has been applied more recently to estimate titanium content across many lunar materials (Lucey *et al.* 1998a, Blewett *et al.* 1997). For mare basalts, this method is quite comparable to the more traditional Charette *et al.* methods.

Plots of the 0.41/0.75-μm ratio against the 1-μm band strength (1.0/0.75-μm ratio) for the units discussed are shown in Fig. 4f. This set of ratios has been commonly used as a "standard" false color composite to examine Clementine and Galileo multispectral images (e.g., Belton *et al.* 1992). In such a "standard" color composite the strength of the 1-μm band absorption as estimated by the VIS/NIR ratio is displayed in green, the UV/VIS ratio in blue and its compliment (VIS/UV) in red.

EASTERN NEARSIDE MARE BASALTS

Tranquillitatis and Serenitatis

Immature crater deposits within northern Tranquillitatis (HDWA) and the central and border regions of Serenitatis (mISP and hDWA, respectivily) have been examined spectrally and compared to mature soils. Study areas within the two basins are shown in Fig. 1. The large crater Dawes (18 km, d in Fig. 1) and a spectrally anomalous region to the west of this crater were excluded from the Tranquillitatis study region since these deposits are believed to include materials excavated from a compositionally distinct subsurface unit (Melendrez *et al.* 1994, Staid and Pieters 1996). The number of craters averaged within each bin and the area of each study region is provided in Table I. Five-color spectra produced by averaging all craters for each size bin are shown in Figs. 3a and 3b. Spectra of mature soils (average of 9×9 pixel homogeneous areas equivalent to 0.81 square kilometers) and the most immature materials are also shown for comparison.

Figure 3a compares the spectral properties of craters in the high titanium basalts of northern Tranquillitatis and the low titanium deposits of central Serenitatis. The spectral properties of craters within these two units were observed to be distinct from one another across all crater sizes sampled. Craters within central Serenitatis' low titanium basalts (Sc) display a diagnostic "red" slope from the ultraviolet to the visible which is similar to mature Serenitatis soils. Immature craters in central Serenitatis also exhibit very strong ferrous absorption features around 1 μm. Since central Serenitatis is often used as a standard area for remote measurements (Pieters and McCord 1976), spectra of central Serenitatis mature soils, 1- to 2-km craters, and the most immature deposits are also shown for comparison with other regions in Figs. 3b, 3c, and 3d. Craters within the high titanium basalts of Tranquillitatis (T) exhibit a much "bluer"

slope from the ultraviolet to the visible similar to mature high titanium soils. The immature craters in both units show an average increase in 1-μm band strength and overall albedo with crater size. However, Tranquillitatis craters are both darker and display a subdued 1-μm absorption relative to Serenitatis craters of similar size.

The mature soils of the Serenitatis border basalts to the northeast have been classified by telescopic studies as hDWA, a bluer unit than the mISP central Serenitatis basalts (Pieters 1978). In Clementine spectra presented in Fig. 3b, mature soils in the Serenitatis border unit (Sb) are slightly bluer and darker than central Serenitatis soils. Immature crater materials from these basalts also appear to be slightly bluer and darker than similar materials in central Serenitatis. The most immature materials in the border (Sb) unit are also bluer and darker and display a weaker 1-μm band.

The spectral properties of the freshest materials in Tranquillitatis and Serenitatis can be compared to laboratory measurements of lunar basalt samples in order to assess the origin of observed spectral differences. Preliminary measurements of a suite of lunar basalt chips with a range in titanium content are shown in Fig. 5. In addition to the prominent ferrous pyroxene absorptions near 1 and 2 μm, significant absorptions also occur at visible and ultraviolet wavelengths in the high-titanium basalt chips (75035,10003; 9–11 wt% TiO_2) but were not observed in the lowest titanium basalt sample (12002,440; <3 wt% TiO_2). These broad absorptions are centered near 0.6 μm and result in a reduced UV/VIS slope for the high titanium samples. Basaltic sample 12063,197, which contains a moderate titanium content (5 wt% TiO_2), exhibits weak absorptions at these visible wavelengths. The measurements of laboratory basalt chips indicate that unweathered high titanium basalts contain absorptions in the visible most likely related to titanium content (Loeffler *et al.* 1975, Burns *et al.* 1976). Although the Clementine wavelengths are limited, these visible absorptions in high-titanium basalts appear to account for some of the distinctions seen between Clementine data for immature craters in high- and low-titanium basalts, but a detailed assessment of such features is beyond the scope of this discussion.

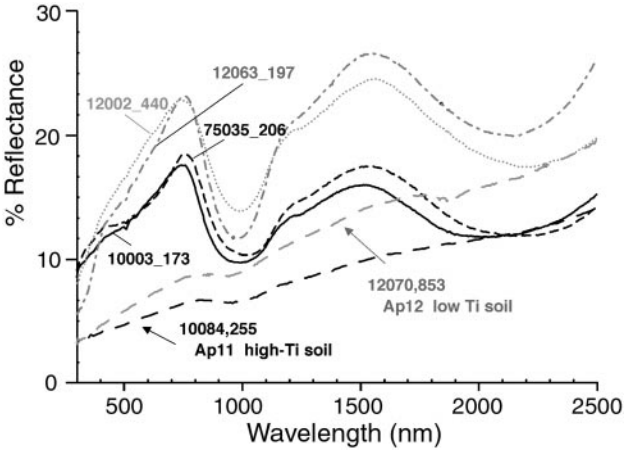

FIG. 5. Laboratory reflectance spectra of lunar basalt chips. Prominent absorptions are observed in high titanium basalts (75035, 10003; 9–11 wt% TiO_2) at visible and ultraviolet wavelengths which are not seen in the low titanium sample (12002,440; <3 wt% TiO_2). Basalt sample 12063, 197 which contains an intermediate titanium content (5 wt% TiO_2) exhibits weak absorptions at these wavelengths. A high titanium Apollo 11 soil and a low titanium Apollo 12 soil are also included in the plot for comparison.

Lacus Somniorum

The Lacus Somniorum region lies outside the northern portion of the Serenitatis basin. The irregular boundaries of this region can be seen in a Clementine 0.75-μm mosaic in Fig. 6. Somniorum's location relative to the larger Serenitatis basin can be seen in Fig. 1. The relatively red and bright mare region of Lacus Somniorum is an example of a mare soil classification which could represent either a compositionally unique basalt type ("LBG-") or a mixture of highland contamination and Serenitatis basalts (Fischer and Pieters 1995).

The central region of Lacus Somniorum has been affected by the presence of a large crater (Danielle, 29 km, 35°N, 31°E), the proximity of Posidonius crater (95 km, 32°N, 30°E), and the embayment of Serenitatis units. As a result, only regions from eastern and western Somniorum outlined in Fig. 6 were used to examine Somniorum materials excavated by small craters. Small Somniorum craters exhibit spectral properties which are distinct from immature crater deposits in the adjacent Serenitatis basin. Optically immature Somniorum materials from three crater size groups <3 km in diameter are compared with similar materials from Serenitatis in Fig. 3c. Notably redder and brighter (in the >0.75-μm region) than the immature materials in Serenitatis, immature craters in Somniorum exhibit a prominent 1-μm ferrous absorption characteristic of basalts. The strength of the ferrous absorption in the Somniorum craters is uniformly weaker than the band exhibited by comparable immature materials in Serenitatis. These characteristics of Sominorium spectra are similar across all crater size groups <3 km in diameter, providing strong evidence that they represent the properties of the basalts emplaced in Sominorium rather than surficial contamination. The weaker 1-μm band observed within the craters of Lacus Somniorum therefore suggests a lower abundance of ferrous minerals in Somniorum basalts relative to the Serenitatis deposits. Craters larger than 3 km were excluded since several exhibit different spectral properties that indicate vertical mixing with underlying feldspathic materials. Such vertical mixing is discussed in the mare–highland mixing section of this paper.

Eastern Mare Frigoris

Like Somniorum, the mare soils of the Frigoris region are relatively bright and red compared to other basalt types on the eastern nearside. Frigoris' deposits extend from Western Procellarum to a region north of Lacus Somniorum and represent the northernmost expanse of basalts on the Moon. The easternmost

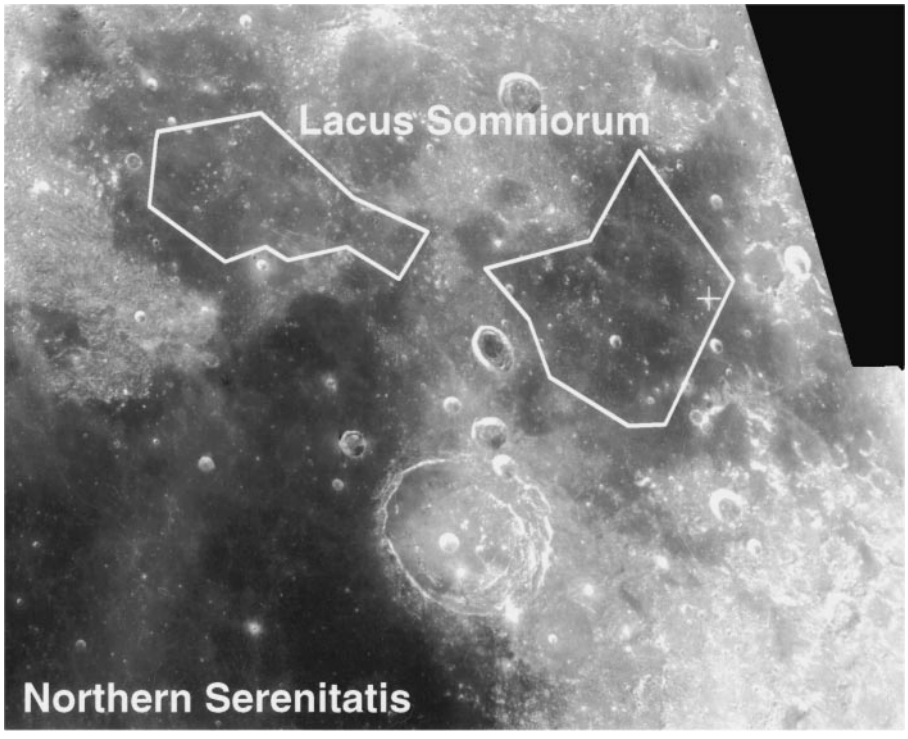

FIG. 6. Clementine 0.75-μm image mosaic of Lacus Somniorum. Areas outlined in white are the locations of the mare study regions from eastern and western Somniorum. The + symbol provides the position of the 3.5-km crater whose spectral properties are plotted in Fig. 4d.

portion of these basalts can be seen in Fig. 1. The majority of the Frigoris deposits have been classified as LBSP by telescopic studies which characterized this mare region as a high albedo, red unit with strong mafic absorptions in the near-infrared (Pieters 1978). Spectra from immature crater groups in Frigoris are compared to central Serenitatis and Somniorum craters in Figs. 3c and 3d. Frigoris crater materials (Fig. 3d) display a high albedo and red UV/VIS slope which are very similar to crater materials in Somniorum for the crater size groups <3 km in diameter. Serenitatis crater materials are less red and bright across all crater size groups. All crater size groups in Frigoris also exhibit very strong 1-μm absorptions. The strength of these absorptions for a given crater size is close to that observed within the Fe-rich low-titanium deposits of central Serenitatis and significantly stronger than craters in Somniorum.

The spectra of the least weathered materials from each mare unit are displayed in Figs. 3e and 3f. The unscaled spectra in Fig. 3e demonstrate that basaltic regoliths in Frigoris are the brightest of those examined and have relatively red UV/VIS spectral properties. A scaled plot of these spectra (Fig. 3f) also demonstrates that the 1-μm absorption feature of Frigoris basalts are similar in strength to central Serenitatis basalts and stronger than the feature observed in other mare types.

The spectral properties of mare Frigoris (Fr) are compared with other basalt regions in Figs. 4a and 4b. As discussed previously, these spectral parameters (0.75-μm albedo and approximate strength of the ferrous absorption band near 1 μm) have been frequently used to estimate maturity and iron content. From Fig. 4, it is easily seen that all of the mare regions (which include very large areas containing mature soils and immature crater materials) plot roughly *parallel* to one another in Figs. 4a and 4b. Furthermore, when comparing two similar basalt types such as Frigoris and Somniorum, the strong 1-μm absorptions in mature soils from Frigoris result in Frigoris soils plotting beneath, but parallel to, mature soils in Somniorum. Fresh materials within the Frigoris region also display a significantly stronger 1-μm band compared to craters in Somniorum with the Frigoris cloud extending to low values of the spectral ratio parameter (1.0/0.75-μm).

Since the small craters of Sominorium and Frigoris are of similar albedos and UV/VIS color, the large difference in ferrous absorption strength cannot result from the masking effects of opaques. There is also no reason to suspect that hundreds of fresh craters in Frigoris are significantly less mature than similarly sized craters in Somniorum. Instead, a compositional control appears to be dominant over the range spectral parameters in Figs. 4a and 4b. It is concluded that the stronger 1-μm bands as measured by the 0.95/0.75- and 1.0/0.75-μm ratios for immature soils in Frigoris represent a higher abundance of iron-bearing minerals such as pyroxenes within the mineralogy of the emplaced basalts. It can also be noted that Somniorum basalts exhibit a very small range across the 0.95/0.75-μm vs 0.75-μm albedo scatter plot. The consistently weak ferrous absorption and the short range across the scatter plots in Figs. 4a and 4b

is an indication of an overall low abundance of iron-bearing pyroxenes for the freshest Somniorum basaltic materials. Such compositional distinctions in abundance of mafic minerals can certainly be made when comparing materials of similar albedo like the basalts of Sominorium and Frigoris. For most basalts, however, a single paramaterization does not capture the diversity of materials affecting albedo and absorption strength.

Application to Stratigraphy and Mare–Highland Mixing

The previous sections describe how Clementine data has been used to characterize the spectral properties of optically immature materials associated with small mare craters. Deposits associated with larger craters may include sites where excavated materials provide information about deeper subsurface deposits. Since craters excavate materials from a depth proportional to their size (Stoffler *et al.* 1975, Dence *et al.* 1977, Grieve *et al.* 1981, Melosh 1989), deposits associated with larger impact craters may be related to the stratigraphy of emplaced basaltic units. Immature deposits associated with several large craters within the eastern lunar nearside have been examined to investigate the thickness of surface units and the composition of underlying materials.

Dawes crater, northern Tranquillitatis. Dawes is a Copernican rayed crater (18 km, 18°N, 26°E) within northern Tranquillitatis near the Serenitatis border (Wilhelms 1987). Its unusual and asymmetric pattern of ejecta supports the hypothesis that Dawes resulted from an east to west oblique impact (Melendrez *et al.* 1994, Staid and Pieters 1996). The location of Dawes relative to the two basins is shown in Fig. 1 by the symbol d. A Clementine 0.75-μm albedo image, a UV/VIS ratio image and a higher resolution Apollo 15 metric frame of Dawes crater are provided in Fig. 7. Compared to surrounding mare materials, lower UV/VIS ratio values were noted for the interior of the crater and in the western ejecta blanket. For example, at a distance of 3.5 km from Dawes, the UV/VIS ratio of mare soils averaged over a 9×9-pixel area (0.81 km^2) was measured to be 0.62 in the west and 0.7 in the east (with standard deviations of 0.008 and 0.006, respectively). Undisturbed mature Tranquillitatis soils further to the east have a ratio value around 0.68 with a standard deviation of 0.005. Based on regional stratigraphy, it has been suggested that the relatively red materials associated with Dawes may represent an underlying layer with a lower titanium content than surficial basalts (Melendrez *et al.* 1994, Staid *et al.* 1996). In previous studies direct compositional interpretation of Dawes and its ejecta was difficult because the relation between mature soils and various immature deposits were poorly defined.

In addition to an asymmetric ejecta pattern, the optical properties of the crater itself exhibits great diversity along the walls. Relatively low albedo and blue wall materials (higher UV/VIS ratio, Fig. 7b) were found in a band around the western interior of the crater while distinctly redder materials (lower UV/VIS ratio) were observed along the eastern wall of the crater and

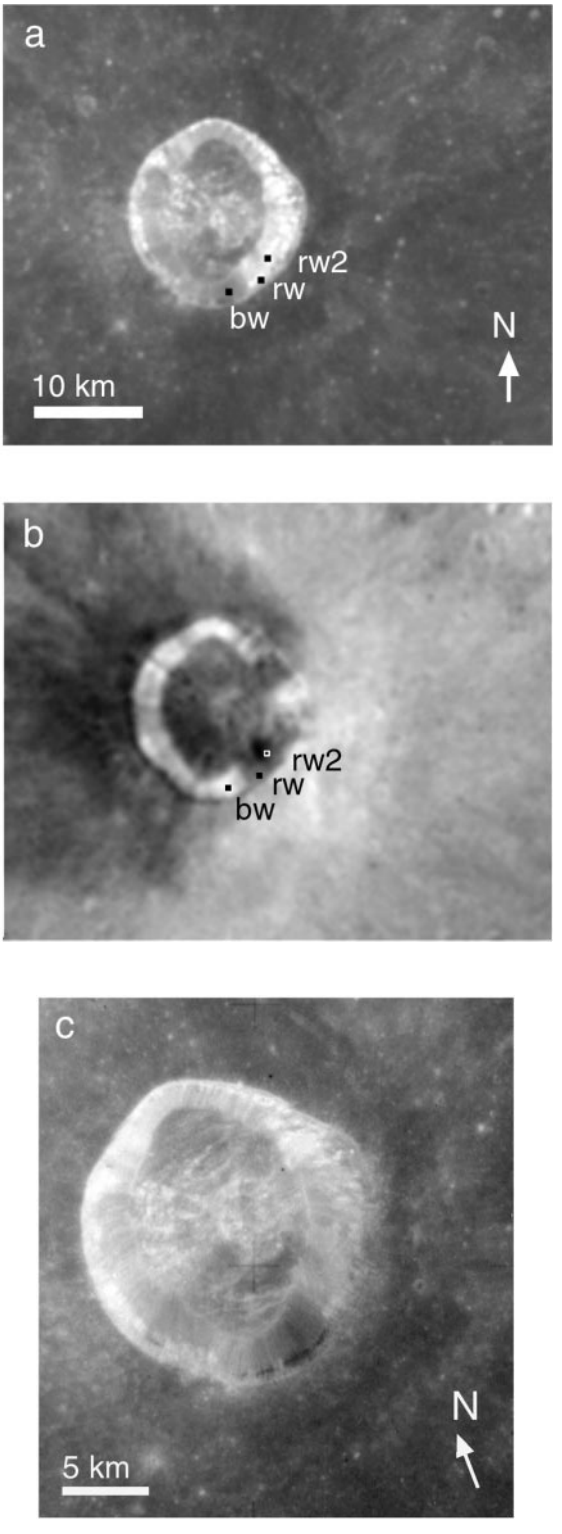

FIG. 7. (a) Clementine 0.75-μm image of Dawes crater (18 km) in northern Mare Tranquillitatis. The locations of 3×3 regions for spectra in Fig. 8 are shown. (b) 0.41/0.75-μm ratio of Dawes crater showing anomalous low values (relatively red) within the western ejecta and portions of the craters interior. (c) Apollo 15 metric of Dawes crater in northern Tranquillitatis (frame 2029). A dark band associated with the exposure and talus wasting of a basalt outcrop can be seen along the interior wall of the crater.

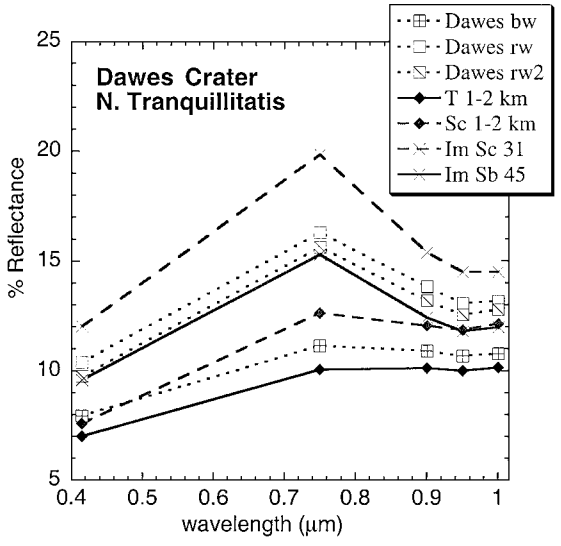

FIG. 8. Five-band Clementine spectra for locations within Dawes crater shown in Fig. 7. Blue wall regions (bw) display properties similar to immature craters within other high-titanium regions of Tranquillitatis (T) while redder wall materials (rw and rw2) are similar to immature deposits in lower titanium Serenitatis (Sb) basalts. Spectra of the three locations sampled in Dawes crater have standard deviations of less than 0.3% reflectance at all wavelengths.

near the crater floor. In order to identify the basalt types exposed within the crater, the spectral properties of these immature deposits within Dawes were compared to those of small immature craters (1–2 km in diameter) within Tranquillitatis and Serenitatis in Fig. 8. The blue wall spectra (bw) is consistent with other fresh materials in Northern Tranquillitatis in its overall albedo, UV/VIS, slope, and band strength. The red wall materials, however, are much brighter and redder and exhibit an increased 1-μm band strength more similar to immature basalts observed in Serenitatis (Sc 1–2 km and Im Sb).

In the higher resolution Apollo 15 metric frame of Dawes crater in Fig. 7c a basalt outcrop within Dawes can also be seen as a distinct band of low albedo materials along the interior crater wall below the southern and western rim. The low albedo blue wall materials (bw) shown in Fig. 8 appear to result from the exposure and talus wasting of this basalt outcrop. These wall materials (bw) also display a subdued 1-μm absorption relative to other areas along the crater wall and are comparable to the spectral properties of surrounding high titanium surface basalts exposed at small craters (T, 1–2 km). It is concluded that the outcrop seen in Fig. 7c is an expression of the high titanium surface units overlain by lower titanium ejecta materials. Spectra of other wall materials (rw) have not been affected by the mass wasting of surface basalts and are distinctly redder. The UV/VIS slope and strength of the 1-μm absorption within the redder deposits are all consistent with the excavation of a buried low-titanium unit. Materials from the lower-titanium subsurface unit were deposited to the west (downrange in the case of an oblique impact), while higher titanium surface basalts were deposited to the east.

Bessel crater, central Serenitatis. Bessel is a 16-km crater that occurs within the low-titanium deposits of central Serenitatis (22°N, 18°E). Its location within Serenitatis is shown in Fig. 1 by the symbol b. Previous studies have identified anomalous and relatively blue ejecta materials surrounding Bessel which suggest the excavation of a higher TiO_2 subsurface unit (Bell and Hawke 1995, Campbell *et al.* 1992). A Clementine 0.75-μm mosaic and UV/VIS ratio image of Bessel crater is shown in Fig. 9. A bright crater ray can be seen crossing to the northwest of Bessel in Fig. 9a. However, the location of the ray suggests that it does not affect the color anomaly associated with the central and eastern crater deposits (Fig. 9b). This relatively blue ejecta was measured in the Clementine images as having a UV/VIS ratio value of 0.64 (2 km southeast of Bessel) while mature Serenitatis soils in this region have a ratio around 0.59 (standard deviations for these ratios are 0.005 and 0.004, respectively).

Clementine five-color spectra of materials within and surrounding Bessel are compared to other materials in Serenitatis in Fig. 10. A typical region of ejecta southeast of Bessel (B ejecta, Fig. 9) exhibits a slightly higher albedo and increased 1-μm absorption strength relative to mature soils in the central and border regions of Serenitatis (m Sc and m Sb). The UV/VIS slope of this ejecta material is also bluer than the central Serenitatis soils and similar to mature soils in the Serenitatis border region. Spectra taken along Bessel's interior walls show variations in 1-μm band strength due to maturity, but only small variations in UV/VIS slope. A very immature area along Bessel's eastern wall (B wall, Fig. 9) is also plotted in Fig. 10 and compared to the most immature materials found in the two Serenitatis study regions (Im Sc and Im Sb). The Bessel wall materials are bluer than other immature materials in central Serenitatis and again are most similar to the slightly darker and bluer immature materials within the Serenitatis border (Sb) basalts to the east. Spectra from both the ejecta and the wall of Bessel suggest the excavation

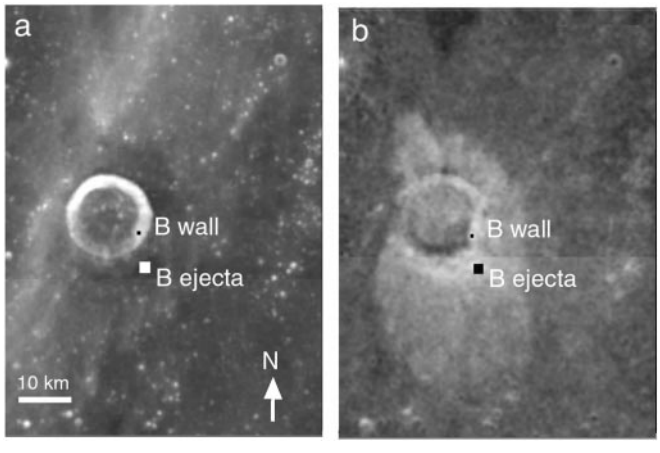

FIG. 9. (a) Clementine 0.75-μm image of Bessel crater (18 km) in central Mare Serenitatis. The locations of regions used to sample spectra shown in Fig. 10 are provided. (b) 0.41/0.75-μm ratio of Bessel crater showing anomalous high values (relatively blue) surrounding the crater.

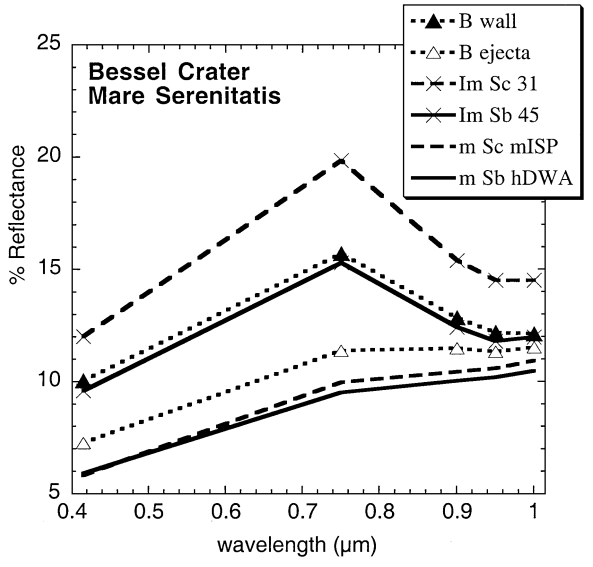

FIG. 10. Five-band Clementine spectra for locations within Bessel crater shown in Fig. 9. The spectral properties of Bessel ejecta (B ejecta) and wall materials (B wall) confirm the excavation of a higher titanium unit similar to mature and immature Serenitatis border (Sb) basalts, respectively. The spectra sampled from Bessel crater have standard deviations of less than 0.4% reflectance at all wavelengths.

of basalts similar in composition to those along the border to the east.

Mare/highland mixing. A variety of data suggest that several regions of the lunar surface in the vicinity of mare/highland morphologic boundaries may have been affected by the mixing of mafic and more feldspathic materials (e.g., Fischer and Pieters 1995, Staid *et al.* 1996, Mustard and Head 1996, Li and Mustard 2000). These zones may result from small to basin-scale impact events, lateral mixing across mare-highland contacts, and vertical mixing of cryptomare and/or mafic intrusions with a thin layer of overlying local highland materials. For several regions of the lunar surface, it is not clear whether the properties of the surface represent the existence of a compositionally distinct unit or the affects of highland mixing with adjacent mare regions.

If there is significant mixing between highland and mare materials, the spectral parameters for such mixtures should fall between those of individual units. In order to examine effects of mare-highland mixing, spectral parameter trends for a variety of areas in Somniorum and surrounding highlands are compared in Fig. 4d. The spectral properties of the mare study region in Somniorum discussed previously (Figure 1 and Table I) are shown in magenta in Fig. 4d for all Somniorum regions excluding craters >2 km. The mature soils and hundreds of small craters (<2 km) within Somniorum fall primarily along a single trend in this parameter space (Sm). This systematic trend represents a range of maturities within the distinct red basalt type in Somniorum. Mature soils and craters within the highlands study area (shown in yellow) exhibit spectral properties which lie along a very different trend in this parameter space (H). The spectral properties associated with a single 3.5-km crater in Somniorum (labeled with + in Fig. 6) are also included in the plot as blue data points and fall between the two compositional trends. The materials within this crater do not exhibit a coherent maturation line, but instead form a mixing trend between Sominorium basalts and highland materials. Materials from this large crater have been disproportionately brightened relative to immature Somniorum basalts by the excavation of feldspathic materials which exhibit spectral properties that deviate from those of uncontaminated basalts in Somniorum. Similarly, this mixed zone contains more mafic-rich materials than highlands (lower 1.0/0.75-μm ratio).

Many of the larger craters within Lacus Somniorum (greater than 3 km in diameter) appear to have excavated more feldspathic material, falling off of the clear maturity trend observed for the smaller craters. The presence of feldspathic materials for many craters in the 3- to 5- and 5+ km size bins indicates that the basalts emplaced within Somniorum are relatively thin (e.g., <500 m in many areas). In several areas, the thin basalts in Lacus Somniorum also contain highland kipukas which can be seen in the Clementine images. The term "kipukas" refers to protruding terra isolated from the rest of their geologic unit by floods of later mare materials (Wilhelms 1987). Highland kipukas are especially abundant near mare–highland contacts as would be expected for thin basalts. It is important to emphasize, however, that for most of Lacus Somniorum, the clear trend in spectral parameters for soils and craters <2 km indicates that vertical mixing with highland material is insignificant except at larger craters.

A deviation from basalt weathering trends and toward highlands is also observed as a bulge in the 1% relative density contour of most mare study areas in Fig. 4c. The most obvious example is seen in the central Serenitatis study region. However, central Serenitatis basalts are known to be relatively thick and vertical excavation of feldspathic materials is not observed, even at the 16-km-diameter Bessel crater. Spatial mapping of this bulge reveals that materials whose spectral properties lie within this region of the scatter plot are associated with several large rays which cross the central Serenitatis study region. Lateral transport of feldspathic materials within these rays is the most likely explanation for their spectral deviation from other areas within the mare study region. The presence of feldspathic materials within rays on the mare surface results in the presence of iron-poor high-albedo materials which alters the maturation trend of emplaced basalts toward that of the highlands.

DISCUSSION AND INTERPRETATIONS

1. Space Weathering of Lunar Basalts

Large areas of several eastern mare units have been examined to characterize the reflectance properties of relatively crystalline mare craters and associated mature soils. Space weathering is observed to alter lunar basalts in a systematic manner which maintains many diagnostic properties, allowing major basalt types

to be distinguished across maturity states. The following observations can be made from the data presented in the previous sections:

1a. The UV/VIS reflectance properties of mare basalts are relatively independent of maturity state and demonstrate only modest reddening as basalt regoliths mature to soils. This is in strong contrast to the significant reddening of feldspathic highlands with maturity. Variations among basalt units are much greater than variations within a unit. This relationship of UV/VIS properties for the units discussed is shown graphically in Figs. 4e and 4f. The UV/VIS properties of immature craters and mature soils from a specific compositional unit are similar to each other and often distinguishable from other units for most basalt types examined.

1b. As mare basalts are exposed to space weathering, a decrease in albedo and the weakening of mafic absorption bands are coupled with the latter being the dominant effect. This alteration process has a similar optical effect across basalt types, resulting in "weathering trends" which are parallel in the 0.75-μm vs 1-μm band strength plots shown in Figs. 4a and 4b. However, feldspathic materials are affected by space weathering differently than basalts, with darkening being the dominant effect. When relatively crystalline feldspathic materials lack a strong ferrous absorption, almost no change is observed in the 1-μm ratio as regoliths weather. Although these materials are observed to darken as a result of weathering (a change in 0.75-μm albedo), a significant change in band strength (0.75/1.0 μm ratio) is often not observed (Figs. 4a and b).

1c. Though basalt weathering trends are parallel in the 0.75-μm vs 1-μm band strength parameter space, basalt types exhibit relative differences in albedo and band strength which are maintained across maturity state resulting in distinct spectral "clouds" for each unit examined. Mare regions where mature soils display relatively strong iron-bearing pyroxene absorptions also exhibit stronger 1-μm absorptions across crater size groups and for the most immature regoliths (Figs. 3e and 3f). Similarly, units with bright mature soils display brighter immature materials across maturity states.

1d. On average, the overall albedo and strength of 1-μm absorptions associated with immature craters of a given unit increase with crater size. It is suggested that larger craters whose deposits have not achieved optical maturity contain a higher proportion of crystalline materials than smaller craters. It is not clear whether differences in crystallinity results from crater morphology (e.g., rate of material erosion downslope) or other factors (e.g., abundance of impact melt) which may affect optical weathering rates.

1e. The high spatial resolution Clementine images have been used to examine the reflectance properties of relatively crystalline crater materials. These materials include a wide range of physical states. Some of the least weathered materials are observed along the walls of steep impact craters and result from the continual mass wasting of wall deposits toward the crater floors. Some small (and presumably very young) craters also exhibit a very high albedo and strong mafic absorption compared to surrounding soils. The least weathered materials observed in this study (Figs. 3e and 3f) display 1-μm absorption bands which are about 30% lower than their reflectance at 0.75 μm outside of the mafic band. The depth of the 1-μm absorption observed in laboratory measurements of "pristine" basalt chips and powders varies with composition and particle size. However, such samples generally display a stronger absorption than is observed remotely. The "pristine" basalt samples in Fig. 5 display 1-μm bands as deep as half of the spectrum's maximum albedo. Some lunar basalt powders display an even stronger 1 μm absorption (e.g., Pieters 1993). Therefore, it is likely that even the most crystalline deposits observed remotely at this resolution (hundreds of meters) are somewhat compromised by the additional presence of more weathered materials.

1f. The eastern high titanium mare units examined in this study display subdued 1-μm absorptions for both mature and the immature mare materials. When compared to the low titanium central Serenitatis basalts, the moderate titanium Serenitatis border unit and the high titanium Tranquillitatis unit exhibit progressively darker crater regoliths with weaker 1-μm bands.

2. Mixing

High-resolution images of small crater deposits allow the spectral properties of materials to be examined which have been excavated from beneath a thin surface veneer containing laterally transported highland materials. Examination of many craters as a function of size has provided an opportunity to identify the effects of vertical mixing of highlands and subsurface mare units. The following implications can be derived from the previous discussion.

2a. As mare basalts weather from regoliths to soils, they display a similar coupling of decreased band strength and darkening. This is different from highland materials, which darken more dramatically. The presence of mare–highland mixing may be identified where the spectral properties of basalts deviate from their coupled darkening and band weakening. The mixing of feldspathic materials with mare basalts results in a new coupling inherent to the mixed materials. The darkening of these materials is anomalous compared nonmixed basalts due to the inclusion of high albedo iron-poor materials. Such mixed materials are offset largely in albedo from nonmixed mare soils from the same region.

2b. Somniorum and Frigoris are two mare regions where interpretation of the basalt composition has been complicated by the possibility of extensive highland mixing. Materials excavated by small craters in Somniorum and eastern Frigoris, however, demonstrate that feldspathic mixing has not been so extensive as to hide the character of emplaced basalts within these regions. Localized regions where highland contamination has occurred exhibit a weakened mafic band and increased albedo.

Such areas include crater rays and larger craters that have excavated submare materials. In Lacus Somniorum vertical nonmare mixing can be identified in local areas for craters in the 3- to 5-km-diameter range, suggesting that basalt deposits are relatively thin (e.g., <500 m) within this region.

2c. Excavation of subsurface highland and mare materials is readily distinguished within the Clementine data. The deposits of central Serenitatis are thick and highland contamination of these basalts appears to be limited to craters closer to the basin's border and several extensive rays. The large crater Bessel (16 km) has excavated a subsurface basalt unit which appears to be slightly higher in titanium content than surface deposits, but there is no evidence that this impact deposited significant highland materials. Dawes crater in Tranquillitatis has excavated a distinctly lower titanium basalt unit from beneath high titanium surface flows. Although the Dawes impact also did not excavate any detectable amount of highland materials, the larger Plinius crater (43 km) to the west did since it displays an increased overall albedo and weakened mafic band indicative of feldspathic materials (Bell and Hawke 1995, Staid *et al.* 1996). Several, somewhat smaller craters elsewhere in the Tranquillitatis basin have also excavated highland material from beneath mare (Staid *et al.* 1996).

3. *Implications for Fe-Mapping Techniques*

The spectral properties of different basalt types have been examined in the spectral-parameter space recently proposed by Lucey *et al.* (1995, 1998a) to estimate FeO and maturity of lunar soils. Many of the results discussed in the previous sections are consistent with general aspects of the Lucey *et al.* approach (1995, 1998a). However, the detailed analysis of mare basalts presented here also identify several important limits to the estimates of FeO and maturity with Clementine spectral parameters.

Plots of the 0.75-μm reflectance vs 1-μm band strength in Figs. 4a and 4b illustrate how changes in band strength and albedo are coupled for the basalt groups examined in this study. Several basalt groups plot in distinct clouds in this parameter space, demonstrating that it is useful for isolating basalts of similar composition across a range of maturity states and identifying *relatively* mature and immature materials within each cloud. The Lucey *et al.* parameters capture relative Fe variations resulting from mare–highland mixing (or mixing of feldspathic highlands with any mafic material). However, our observations suggest that the Lucey *et al.* proposed rotational analysis of the data clouds should not be directly interpreted in terms of %Fe for *mare* units based on the observations summarized below. Furthermore, though relative differences in maturity within a unit can be identified by comparing the 0.75-μm albedo and 1-μm band strengths of materials within a single basalt group, our results indicate that the absolute maturity of mare materials cannot be compared across units without addressing spectral properties resulting from several differences in mineral composition, largely pyroxene and opaque abundance.

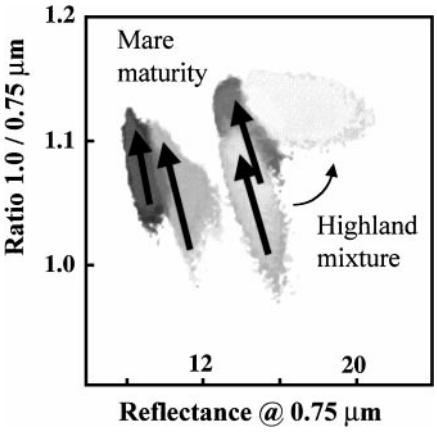

FIG. 11. Proposed basalt weathering trends within the 1.0/0.75-μm vs 0.75-μm reflectance parameter space for the mare units examined. Basalt weathering trends are roughly parallel within this parameterization and offsets and differences in range along the maturity line vary as a result of compositional differences. Rotational deviations from parallel trends result from mixing of mafic-rich (mare) material with feldspathic materials.

3a. Large regions of different mare basalt types show a similar trend of decreased albedo and 1-μm band strength with increasing maturity resulting in parallel clouds within the 0.75-μm vs 1-μm band strength plots. A rotational trend dependent upon composition is not observed in Figs. 4a and 4b where large regions of different basalt types are compared which contain a full range of optical maturities. Figure 11 presents an alternate interpretation for basalt weathering trends which are roughly parallel in this parameter space. Offsets and ranges along the maturity line vary as a result of compositional differences. For mare basalts, rotational spectral properties observed in this parameter space results from feldspathics mixing with a specific basalt composition. Although mare are all FeO-rich in an absolute sense, the rotational spectral parameter method does not capture some of the more subtle variations in FeO content among mare basalt types. Such compositional variations between mare regions are observed spectrally for materials with the same optical maturity and opaque content but different ferrous band strengths.

3b. The absolute position of the parameter described by Lucey *et al.* (1998a,b) as "maturity" (roughly, the radial distance from a point in the upper left of Figs. 4a and 4b) is affected by the compositional properties of the emplaced basalts, such as amount of ilmenite opaques and Fe-bearing pyroxenes. This dependence can be observed as offsets between mature soils in the spectral parameter space for large regions of different mare types in Figs. 4a and 4b. For example, mature soils throughout Frigoris plot below mature soils in Somniorum because they contain a higher abundance of Fe-bearing minerals, not because they are more immature. For the same reason, immature materials in Frigoris display a much larger range along the axis of the data cloud than deposits in Somniorum. Materials within Serenitatis and Tranquillitatis also demonstrate a difference in

the absolute value for mature soils and range of values in the spectral parameters of Figs. 4a and 4b. Since large areas of the Moon containing many craters should contain materials with similar maturity states, this optical effect must result from *compositional* differences between basalt types rather than differences in surface age, or optical maturity. The position of mare surface material along the axis of the data cloud for that unit provides a good estimate of its relative maturity (e.g., Fig. 11) but does not provide information for direct comparison with other units.

COMPOSITION OF EASTERN NEARSIDE MARIA

The mare basalts of the Tranquillitatis and Serenitatis regions are some of the most well studied on the Moon and contain mare units with known differences in titanium content. These regions allow immature mare materials to be compared to mature soils across units with established compositional differences. By comparison, the spectral properties of Lacus Somniorum and Mare Frigoris have previously led to varied interpretations of basalt composition. The mare deposits of these two northern mare regions provide an interesting comparison since both Lacus Somniorum and Mare Frigoris contain soils and crater materials which are unusually red and bright but exhibit very different ferrous absorption bands. The compositional properties of these basalts are re-evaluated below based on previous research (e.g., Pieters 1978, Johnson *et al.* 1991a, Melendrez *et al.* 1994, Bell and Hawke 1995, Staid *et al.* 1996, Lucey *et al.* 1998a, Hiesinger *et al.* 1998) and results presented here. Discussions of the optical properties of each basalt type are followed by a comparison of the compositional properties of all five basalt groups.

Mare Tranquillitatis (T). Previous studies have identified at least four basalt types within the Tranquillitatis basin ranging from low titanium flows in the northeast to the very high titanium units which dominate the basin. The youngest very high titanium flows are the only two basalt groups included here in the Tranquillitatis study area. Most of the study region lies within an extensive very high titanium unit ($T_{\text{vh-B}}$; Staid *et al.* 1996) and corresponds to the majority of blue (high 415/750) Tranquillitatis materials plotted in Fig. 4e. Bulk soils within this region have been mapped as containing 5–8% titanium content (Melendrez *et al.* 1994). The volcanic event that produced these extensive flows are likely to have been be the source of the low-K high-Ti Apollo samples (~10% TiO_2; 3.67–3.71 Ga) at both the Apollo 11 and the Apollo 17 landing sites (Staid *et al.* 1996). The southern portion of the study region includes a small area of the youngest mare unit in Tranquillitatis ($T_{\text{vh-A}}$; Staid *et al.* 1996) believed to include the most titanium rich mare soils observed on the lunar surface (Melendrez *et al.* 1994, Johnson *et al.* 1991a). A link between these basalts and the high titanium samples (~11% TiO_2, 3.59 Ga) collected at Apollo 11 landing site has been suggested based on stratigraphic relations and their spatial distribution (Staid *et al.* 1996). The reflectance properties of these high titanium mare materials result in the bluest (highest 0.41/0.75-μm ratio) materials observed in Fig. 4e. The single immature 3- to 5-km crater identified in the Tranquillitatis study area also occurs within this southern titanium-rich region. This crater, which is plotted in Fig. 3a, also has bluer UV/VIS properties than the other immature crater groups within Tranquillitatis.

The immature mare deposits associated with Dawes crater suggest that the very high titanium units ($T_{\text{vh-B}}$) are less than 2 km thick in the northern portion of Tranquillitatis and overlay a lower titanium unit. These low-titanium materials are most likely linked to the stratigraphically older low-titanium deposits observed elsewhere in the Tranquillitatis basin (Melendrez *et al.* 1994, Staid *et al.* 1996). The low-titanium materials observed within Dawes crater are spectrally similar to the basalts observed along the eastern border of Serenitatis. However, it is unlikely that these two deposits are related in time because the Serenitatis border unit appears to be younger than the most recent Tranquillitatis events (Carr 1966, Wilhelms 1987, Hiesinger *et al.* 1998).

Mare Serenitatis border (Sb). The basalts along the eastern border of Serenitatis (hDWA basalts in the Pieters (1978) classification) are bounded by the northernmost high titanium Tranquillitatis flows to the south and the low titanium Serenitatis flows to the west. Figure 4e demonstrates that soils within this border unit are slightly bluer (high 415/750) and darker than central Serenitatis flows but considerably redder (lower 415/750) and brighter than the very high titanium basalts within Tranquillitatis. Soil composition is expected to be 2–5% TiO_2.

Central Mare Serenitatis (Sc). The basalts within central Serenitatis have previously been interpreted as low titanium (<4% TiO_2) and high iron basalts based on the optical properties of their mature soils as well as Apollo γ-ray orbital data. The optical properties of crater materials within the central Serenitatis basalts provide information consistent with this composition. These basalts exhibit redder UV/VIS properties and a stronger 1-μm band than craters in Tranquillitatis. Previous work has identified deposits surrounding Bessel crater which may contain somewhat higher titanium basalts from a buried mare unit (Campbell *et al.* 1992, Bell and Hawke 1995). Examination of immature mare materials associated with Bessel suggests that this buried unit is similar in composition to the basalts along the eastern border of Serenitatis discussed above.

Lacus Somniorum (Sm). As shown in Fig. 4e, the basalts within Lacus Somniorum are much redder (low 415/750) and brighter than the deposits in Mare Serenitatis. Small immature craters within Somniorium exhibit a distinct 1-μm absorption indicative of iron-bearing silicates such as pyroxene and olivine which are common essential constituents of basalts. The consistency of this absorption across size groups of small craters indicates these are properties of the emplaced basalt and not contamination with highlands. These basalts must contain a very low amount of opaques and a relatively large abundance of high albedo components (e.g., plagioclase) as their albedo is close

to that of mature highland soils. The red (low 415/750) optical properties of these basalts are also consistent with a very low ilmentite content and their inferred TiO_2 is thus certainly <2%, and probably <1%. The strength of the 1-μm ferrous absorption is also consistently weak compared to other mare basalts, indicating that these are low iron basalts. Local regions within these thin basalts are also observed to contain highland mixing and optical data for such mixed regions fall between the weathering trends of basalts and highlands.

Eastern Mare Frigoris (Fr). The UVVIS spectral properties of eastern Mare Frigoris are similar to those of Lacus Somniorum, suggesting the deposition of another low to very low titanium mare unit. Like Somniorum, immature crater deposits within the Frigoris basalts demonstrate consistent spectral properties that result from the composition of emplaced basalts rather than highland contamination. Both mare deposits contain relatively low abundances of opaques and ilmenite as indicated by their similar albedos and UV/VIS spectral properties. However, Frigoris basalts also display a strong ferrous absorption band at 1 μm (the strongest of all basalts studied here) for both mature soils and immature crater ejecta. Therefore, Frigoris basalts must have a higher abundance of iron-bearing minerals (and thus a higher iron content) than Somniorum basalts. Though the strong mafic band observed within Frigoris basalts indicates a higher abundance of iron bearing minerals than Somniorum, the two regions exhibit a similar albedo. A correlation between iron content and albedo was observed by Lucey *et al.* (1998a) for measurements of lunar glasses and a variety of minerals. Mare Frigoris and Mare Somniorum, although both basaltic, provide an example where small differences in mineralogy (e.g., opaque distribution, particle size, and abundance) can cause deviation from this trend. For example, assuming both have low abundances of ilmenite, Somniorum ilmenite occuring as finer particles would compensate for the lower abundance of Fe-bearing silicates. Future high-resolution Lunar Prospector data may provide additional insight into the unusual spectral properties of these two mare assemblages.

The ferrous band strength of small craters in Frigoris is similar to that of the high iron central Serenitatis basalts (Figs. 4a, 4b). However, central Serenitatis basalts are darker and are likely to include more absorbing materials than Frigoris basalts. The strength of absorption features will be subdued more in basalts with increased opaques than in basalts containing less opaques. Following this logic leads to the conclusion that though Frigoris basalts are higher in iron content than Somniorum basalts they must be lower in iron content than central Serenitatis basalt to exhibit a similar band strength. Similarly, Tranquillitatis basalts contain much more opaques than Somniorum basalts but exhibit similar band strengths. Therefore, Tranquillitatis basalts also contain more iron than Somniorum basalts.

Elemental abundance estimates. A summary of estimated iron and titanium content can be made for the five mare basalts discussed here (T, Sb, Sc, Sm, Fr). For completeness, we compare the results presented in the previous sections with the spectral parameter method of Lucey *et al.* (1998a). Even though the approach taken here emphasizes mineralogical properties and differences, our results can be compared in a relative sense with those of Lucey *et al.* In some cases, the estimates are necessarily nonunique. There is good agreement in the spectral methods for estimating TiO_2 for mare basalts, but some disagreement for FeO.

The relative titanium content of mare basalts estimated using the modified Charette *et al.* "spectral contrast" approach (e.g., Johnson *et al.* 1991b, Pieters 1993) is quite similar to the Lucey *et al.* estimate for mare basalts (high to low): TiO_2: T > Sb > Sc ≥ (Fr, Sm). On the other hand, for our mineralogy-based assessment, the relative iron content of the basalts is (high to low):

$$\text{FeO [mineralogy]: Sc} > \text{Fr} > \text{Sm; and (T, Sb)} > \text{Sm.}$$

Whereas using the spectral parameter approach of Lucey *et al.* (1998a), the estimated iron content for mare basalts would be different:

$$\text{FeO [Lucey } et\ al.\text{]: T} > \text{(Sb, Sc)} > \text{(Fr, Sm).}$$

We note that the spectral paramater approach can provide a good first-order estimate of iron content: materials with abundant mafic minerals can be readily distinguished from those dominated by anorthosite, and mixtures fall between the two. Because of the more complex interplay of different Fe-bearing minerals (and weathering effects) on optical properties, the Lucey *et al.* parameter approach cannot resolve several ambiguities among basalt types, all of which are mafic-rich lithologies. The roughly parallel nature of the parameter data clouds for each basalt type in Fig. 4, and the notable offset of each basalt from any simple rotational mixing line, is a result of their multivariant mineralogy. The observed offsets of weathering trends of individual basalt units using the band strengths and albedo parameters contain additional information about the spectral and mineralogical differences between mare regions.

Overall, the relatively crystalline deposits associated with mare craters have demonstrated important new information for the remote analysis of lunar volcanics. Initial results presented here complement previous studies of several nearside basalt types with new insight into the interpretation of mare basalt composition and stratigraphy. Future studies will expand this approach to compare basalt types examined here with western and farside lunar volcanics.

ACKNOWLEDGMENTS

The authors acknowledge support for this research from NASA Grants NAG5-4366 and NAGW-5101. We thank J. Johnson and L. Keller for thoughtful and helpful reviews of the original manuscript.

REFERENCES

Adams, J. B. 1974. Visible and near-infrared reflectance spectra of pyroxenes as applied to remote sensing of solid objects in the Solar System. *J. Geophys. Res.* **79**, 4829–4836.

Adams, J. B., F. Horz, and R. V. Gibbons 1979. Effects of shock-loading on the reflectance spectra of plagioclase, pyroxene, and glass. *Lunar Planet. Sci. Conf. 10th*, 1–3. [Abstract]

Adams, J. B., T. B. McCord, C. M. Pieters, C. R. Chapman, A. E. Metzger, T. V. Johnson, I. Adler, and M. J. Bielefeld 1981. Remote sensing of basalts in the Solar System. In *Basaltic Volcanism on the Terrestrial Planets* (Basaltic Volcanism Study Project), pp. 438–490. Pergamon, New York.

Bell, J., and B. Hawke 1995. Compositional variability of the Serenitatis/Tranquillitatis region of the Moon from telescopic multispectral imaging and spectroscopy. *Icarus* **118**, 51–68.

Belton, M. J., J. W. Head, C. M. Pieters, R. Greeley, A. S. McEwen, G. Neukum, K. P. Klaasen, C. D. Anger, M. H. Carr, C. R. Chapman, M. E. Davies, F. P. Fanale, P. J. Gierasch, R. Greenberg, A. P. Ingersoll, T. V. Johnson, B. Paczkowski, C. B. Pilcher, and J. Veverka 1992. Lunar impact basins and crustal heterogeneity: New western limb and far side data from Galileo. *Science* **255**, 570–576.

Blewett, D. T., P. G. Lucey, B. R. Hawke, and B. L. Jolliff 1997. Clementine images of lunar sample return stations; refinement of FeO and TiO_2 mapping techniques. *J. Geophys. Res.* **102**, 16,319–16,325.

Burns, R. G. 1993. Origin of electronic spectra of minerals in the visible to near-infrared region. In *Remote Geochemical Analysis: Elemental and Mineralogical Composition* (C. Pieters and P. Englert, Eds.), pp. 3–27. Cambridge Univ. Press, Cambridge, UK.

Burns, R. G., K. M. Parkin, B. M. Loeffler, I. S. Leung, and R. M. Abu-Eid 1976. Further characterization of spectral features attributable to titanium on the Moon. *Proc. Lunar Sci. Conf. 7th*, 2561–2578.

Campbell, B. A., J. F. Bell III, S. H. Zisk, B. R. Hawke, and K. A. Horton 1992. A high resolution radar and CCD imaging study of crater rays in Mare Serenitatis and Mare Nectaris. *Proc. Lunar Planet. Sci. Conf. 22nd*, 259–274.

Carr, M. H. 1966. *Geologic Map of the Mare Serenitatis Region of the Moon*, USGS Map I-489 (LAC-42), scale 1:1,000,000.

Charette, M. P., T. B. McCord, C. M. Pieters, and J. B. Adams 1974. Application of remote spectral reflectance measurements to lunar geology classification and determination of titanium content of lunar soils. *J. Geophys. Res.* **79**, 1605–1613.

Cloutis, E. A., and M. J. Gaffey 1991. Pyroxene spectroscopy revisited: Spectral–compositional correlations and relationship to geothermometry. *J. Geophys. Res.* **96**, 22,809–22,826.

Davis, P. A. 1980. Iron and titanium distribution on the Moon from orbital gamma ray spectrometry with implications for crustal evolutionary models. *J. Geophys. Res.* **85**, 3209–3224.

DeHon, R. A., and J. D. Waskom 1976. Geologic structure of the eastern mare basins. *Proc. Lunar Sci. Conf. 7th*, 2729–2746.

Dence, M. R., R. A. F. Grieve, and P. B. Robertson 1977. Terrestrial impact structures: Principal characteristics and energy considerations. In *Impact and Explosion Cratering: Planetary and Terrestrial Implications* (D. J. Roddy, R. O. Pepin and R. B. Merrill, Eds.), pp. 247–275. Pergamon, New York.

Fischer, E. M., and C. M. Pieters 1995. Lunar surface aluminum and iron concentration from Galileo SSI data, and the mixing of mare and highland materials. *J. Geophys. Res.* **100**, 23,279–23,290.

Fischer, E. M., and C. M. Pieters 1996. Composition and exposure age of the Apollo 16 Cayley and Descartes regions from Clementine Data: Normalizing the optical effects of space weathering. *J. Geophys. Res.* **101**, 2225–2234.

Greeley, R., S. D. Kadel, D. A. Williams, L. R. Gaddis, J. W. Head, A. S. McEwen, S. L. Murchie, E. Nagel, G. Neukum, C. M. Pieters, J. M. Sunshine, R. Wagner, and M. J. S. Belton 1993. Galileo imaging observations of lunar maria and related deposits. *J. Geophys. Res.* **98**, 17,183–17,205.

Grieve, R. A. F., P. B. Robertson, and M. R. Dence 1981. Constraints on the formation of ring impact structures, based on terrestrial data. *Proc. Lunar Planet. Sci. Conf. 12th*, 37–57.

Head, J. W. 1976. Lunar volcanism in space and time. *Rev. Geophys. Space Phys.* **14**, 265–300.

Head, J. W., and L. Wilson 1992. Lunar mare volcanism: Stratigraphy, eruption conditions, and the evolution of secondary crusts. *Geochim. Cosmochim. Acta* **55**, 2155–2175.

Hiesinger, H., R. Jaumann, G. Neukum, and J. W. Head 1996. Mare Australe: New results from Lunar Orbiter and Clementine UV/VIS imagery. *Lunar Planet. Sci. Conf. 27th*, 545–546. [Abstract]

Hiesinger, H., R. Jaumann, G. Neukum, and J. W. Head 1998. Ages of lunar mare basalts. *Lunar Planet. Sci. Conf. 29th*, 1242. [Abstract]

Horz, F. 1978. How thick are the lunar mare basalts? *Proc. Lunar Planet. Sci. Conf. 9th*, 3311–3331.

Howard, K. A., M. H. Carr, and W. R. Muehlberger 1973. *Basalt Stratigraphy of Southern Mare Serenitatis*, Stratigraphc Studies 29, Apollo 17 Preliminary Science Report, NASA Report SP-330, pp. 29.1–29.12. U.S. Govt. Printing Office, Washington, DC.

Johnson, J. R., S. M. Larson, and R. Singer 1991a. Remote sensing of potential lunar resources, 1, Near side compositional properties. *J. Geophys. Res.* **96**, 18,861–18,882.

Johnson, J. R., S. M. Larson, and R. B. Singer 1991b. A Reevaluation of spectral ratios for lunar mare TiO_2 mapping. *Geophys. Res. Lett.* **18**, 2153–2156.

Johnson, T.V., R. S. Saunders, D. L. Matson, and J. A. Mosher 1977. A TiO_2 abundance map for the northern maria. *Lunar Planet. Sci. Conf. 8th*, 1029–1036.

Kadel, S. D., and R. Greeley 1992. Mare basalts in the Orientale Basin; Galileo multispectral observations. *Lunar Planet. Sci. Conf. 23rd*, 647–648. [Abstract]

Lawrence, D. J., W. C. Feldman, B. L. Barraclough, A. B. Binder, R. C. Elphic, S. Maurice, and D. R. Thomsen 1998. Global elemental maps of the Moon: The Lunar Prospector gamma-ray spectrometer. *Science* **281**, 1484–1489.

Li, L., and J. F. Mustard 2000. Compositional gradients across mare-highland contact: The importance and geological implication of lateral mixing. *J. Geophys. Res.*, in press.

Loeffler, B. M., R. G. Burns, and J. A. Tossell 1975. Metal → metal charge transfer transitions: Interpretation of visible-region spectra of the Moon and lunar materials. *Proc. Lunar Planet. Sci. Conf. 6th*, 2663–2676.

Lucey, P. G., D. T. Blewett, and B. R. Hawke 1998a. Mapping the FeO and TiO_2 content of the lunar surface with multispectral imagery. *J. Geophys. Res.* **103**, 3679–3699.

Lucey, P. G., G. J. Taylor, and B. R. Hawke 1998b. Global imaging of maturity: Results from Clementine and lunar sample studies. *Lunar Planet. Sci. Conf. 29th* [Abstract].

Lucey, P. G., G. J. Taylor, and E. Malaret 1995. Abundance and distribution of iron on the Moon. *Science* **268**, 1150–1153.

Matson, D. L., T. V. Johnson, and G. J. Veeder 1977. Soil maturity and planetary regoliths: The Moon, Mercury, and the asteroids. *Proc. Lunar Planet. Sci. Conf. 8th*, 1001–1012.

McCord, T. B., and J. B. Adams 1973. Progress in remote optical analysis of lunar surface composition. *Moon* **7**, 453–474.

McCord, T. B., C. M Pieters, and M. A Feierberg 1976. Multispectral mapping of the lunar surface using groundbased telescopes. *Icarus* **29**, 1–34.

McCord, T. B., R. N. Clark, B. R. Hawke, L. A. McFadden, P. D. Owensby, C. M. Pieters, and J. B. Adams 1981. Moon: Near-infrared spectral reflectance, a first good look. *J. Geophys. Res.* **86**, 10,883–10,892.

McCord, T. B., M. Grabow, M. A. Teierberg, D. MacLaskey, and C. M. Pieters 1979. Lunar multispectral maps: Part II of the lunar nearside. *Icarus* **37**, 1–28.

McEwen, A., E. Eliason, P. Lucey, E. Malaret, C. Pieters, M. Robinson, and T. Sucharski 1998. Summary of radiometric calibration and photometric normalization steps for the Clementine UVVIS images. *Lunar Planet. Sci. Conf. 29th*, 1466. [Abstract]

Melendrez, D. E., J. Johnson, S. Larson, and R. Singer 1994. Remote sensing of potential lunar resources 2. High spatial resolution mapping of spectral reflectance ratios and implications for near side mare TiO_2 content, *J. Geophys. Res.* **99**, 5601–5620.

Melosh, H. J. 1989. *Impact Cratering.* Oxford Univ. Press, New York.

Merenyi, E, A. S. McEwen, M. S. Robinson, and R. A. Craddock 1997. Spectral mapping of Mare Mosciviense, lunar farside, from Clementine UVVIS data. *Lunar Planet. Sci. Conf. 28th*, 939–940. [Abstract]

Metzger, A. E., and R. E. Parker 1979. The distribution of titanium on the lunar surface. *Earth Planet. Sci. Lett.* **45**, 155–171.

Mustard, J. F., and J. W. Head 1996. Mare-highland mixing relationships along the southwestern shores of Oceanus Procellarum. *J. Geophys. Res.* **101**, 18,913–18,925.

Nozette, S., P. Rustan, L. P. Pleassance, D. M. Horan, P. Regeon, E. M. Shoemaker, P. D. Spudis, C. H. Acton, D. N. Baker, J. E. Blamont, B. J. Buratti, M. P. Corson, M. E. Davies, T. C. Duxbury, E. M. Eliason, B. M. Jakosky, J. F. Kordas, I. T. Lewis, C. L. Lichenberg, P. G. Lucey, E. Malaret, M. A. Massie, J. H. Resnick, C. J. Rollins, H. S. Park, A. S. McEwen, R. E. Priest, C. M. Pieters, R. A. Reisse, M. S. Robinson, R. A. Simpson, D. E. Smith, T. C. Sorenson, R. W. Vorder Bruegge, and M. T. Zuber 1994. The Clementine mission to the Moon: Scientific overview. *Science* **266**, 1835–1839.

Pieters, C. M. 1978. Mare basalt types on the front side of the Moon: A summary of spectral reflectance data. *Proc. Lunar Planet. Sci. Conf. 9th*, 2825–2849.

Pieters, C. M. 1993. Compositional diversity and stratigraphy of the lunar crust derived from reflectance spectroscopy. In *Remote Geochemical Analysis: Elemental and Mineralogical Composition* (C. Pieters and P. Englert, Eds.), pp. 309–339. Cambridge Univ. Press, Cambridge, UK.

Pieters, C. M., and T. M. McCord 1976. Characterization of lunar mare basalt types. I. A remote sensing study using reflection spectroscopy of surface soils. *Proc. Lunar Sci. Conf. 7th*, 2677–2690.

Pieters, C. M., G. He, M. Staid, S. Tompkins, and E. Fischer 1995b. Clementine UVVIS data calibration and processing. http://www.planetary.brown.edu/clementine/calibration.html. Online: August, 1995, last update, March 1997.

Pieters, C. M., J. W. Head, J. B. Adams, T. B. McCord, S. H. Zisk, and J. L. Whitford-Stark 1980. Late high-titanium basalts of the western maria: Geology of the Flamsteed region of Oceanus Procellarum. *J. Geophys. Res.* **85**, 3913–3938.

Pieters, C. M., M. I. Staid, E. M. Fischer, and G. He 1994. A sharper view of impact craters from Clementine data. *Science* **266**, 1844–1848.

Pieters, C. M., G. He, S. Tompkins, M. Staid, E. M. Fischer 1995a. The low-Ti basalts of Tsiolkovsky as seen by Clementine. *Lunar Planet. Sci. Conf. 26th*, 1121–1122. [Abstract]

Robinson, M. S., B. R. Hawke, P. G. Lucey, and G. A. Smith 1992. Mariner 10 multispectral images of the eastern limb and farside of the Moon. *J. Geophys. Res.* **97**, 18,265–18,274.

Schaber, G. G. 1973. Lava flows in Mare Imbrium: Geologic evaluation from Apollo orbital photography. *Proc. Lunar Planet. Sci. Conf. 4th*, 73–92.

Sjogren, W. L., R. N. Wimberly, and W. R. Wollenhaupt 1974. Lunar gravity via the Apollo 15 and 16 subsatellites. *Moon* **9**, 115–128.

Snyder, G. A., L. A. Taylor, and C. R. Neal 1992. A chemical model for generating the sources of mare basalts: Combined equilibrium and fractional crystallization of the lunar magmasphere. *Geochim. Cosmochim. Acta* **56**, 3809–3823.

Snyder, G. A., D Lee, L. A. Taylor, A. Halliday, and A. Jerde 1994. Evolution of the upper mantle of the Earth's Moon: Nd and Sr isotopic constraints from high-Ti mare basalts. *Geochim. Cosmochim. Acta* **58**, 4795–4808.

Solomon, S. C., and J. W. Head 1980. Lunar mascon basins: Lava filling, tectonics and evolution of the lithosphere. *Rev. Geophys. Space Phys.* **18**, 107–141.

Staid, M. I., and C. M. Pieters 1996. Craters as indicators of basalt straigraphy in Mare Tranquillitatis and Serenitatis. *Lunar Planet. Sci. Conf. 27th*, 1259–1260. [Abstract]

Staid, M. I., C. M. Pieters, and J. W. Head 1995. A multispectral view of stratigraphy in Mare Tranquillitatis. *Lunar Planet. Sci. Conf. 26th*, 1345–1346. [Abstract]

Staid, M. I., C. M. Pieters, and J. W. Head III 1996. Mare Tranquillitatis: Basalt emplacement history and relation to lunar samples. *J. Geophys. Res.* **101**, 23,213–23,228.

Stoffler, D., D. E. Gault, J. A. Wedekind, and G. Polkowski 1975. Experimental hypervelocity impact into quartz sand: Distribution and shock metamporphism of ejecta. *J. Geophys. Res.* **80**, 4062–4077.

Taylor, G. J., P. G. Lucey, B. R. Hawke, and P. D. Spudis 1996. Composition of the lunar maria. *Lunar Planet. Sci. Conf. 27th*, 1317–1318. [Abstract]

Wilhelms, D. E. 1987. *The Geologic History of the Moon*, United States Geological Survey Professional Paper 1348. USGS, Washington, DC.

Williams, D. A., R. Greeley, G. Neukum, and R. Wagner 1993. Multispectral studies of selected crater- and basin-filling lunar maria from Galileo Earth–Moon encounter 1. *Lunar Planet. Sci. Conf. 24th*, 1521–1522. [Abstract]

Zuber, M. T., D. E. Smith, F. G. Lemoine, and G. A. Neumann 1994. The shape and internal structure of the Moon from the Clementine Mission. *Science* **266**, 1839–1843.